Strain-induced semiconductor to metal transition in MA_2Z_4 bilayers (M = Ti, Cr, Mo; A = Si; Z = N, P)

Hongxia Zhong [1,2] Wenqi Xiong,[2] Pengfei Lv,[2] Jin Yu [3,4,*] and Shengjun Yuan [2,†]

[1]*School of Mathematics and Physics, China University of Geosciences (Wuhan), Wuhan 430074, China*
[2]*School of Physics and Technology, Wuhan University, Wuhan 430072, People's Republic of China*
[3]*Shanghai Key Laboratory of Mechanics in Energy Engineering, Shanghai Institute of Applied Mathematics and Mechanics,*
School of Mechanics and Engineering Science, Shanghai University, Shanghai 200444, China
[4]*Institute for Molecules and Materials, Radboud University, Heijendaalseweg 135, NL-6525 AJ Nijmegen, Netherlands*

Very recently, a new type of two-dimensional layered material, $MoSi_2N_4$, was fabricated that is semiconducting with weak interlayer interaction, high strength, and excellent stability. We systematically investigate the effect of vertical strain on the electronic structure of MA_2Z_4 (M = Ti/Cr/Mo, A = Si, Z = N/P) bilayers. Taking bilayer $MoSi_2N_4$ as an example, our first-principles calculations show that its indirect band gap decreases monotonically as the vertical compressive strain increases. Under a critical strain around 22%, it undergoes a transition from semiconductor to metal. We attribute this to the opposite energy shift of states in different layers, which originates from the built-in electric field induced by the asymmetric charge transfer between two inner sublayers near the interface. Similar semiconductor to metal transitions are observed in other strained MA_2Z_4 bilayers, and the estimated critical pressures to realize such transitions are within the same order as semiconducting transition metal dichalcogenides. The semiconductor to metal transitions in the family of MA_2Z_4 bilayers present interesting possibilities for strain-induced engineering of their electronic properties.

I. INTRODUCTION

The family of two-dimensional (2D) materials has attracted great interest since the exfoliation of monolayer graphene from graphite [1,2]. They have many unique properties and distinguished performance in applications, including mechanical engineering, electronics, and information and energy technologies [3–8]. Motivated by this, theorists have continuously proposed many new 2D materials with excellent physical or chemical properties [9–13]. However, only a few of these materials have been synthesized successfully in monolayers [14–19], and they are mostly lamellar in their natural bulk forms, with the component layers assembled by weak van der Waals interaction. Recently, research enthusiasm was extended to those 2D materials whose bulk forms are not layered in nature. A typical example is the hexagonal MXenes family, which was fabricated by etching out the A layers from MAX materials [20–22]. In a very recent work, $MoSi_2N_4$, as a member of another new family of 2D molybdenum nitrides [23,24], was successfully grown by the chemical vapor deposition method [20]. It is reported to be semiconducting with high strength and remarkable stability [20]. Since multilayer $MoSi_2N_4$ is stacked by very weak van der Waals interaction, it is structurally flexible and easy to deform. Meanwhile, it is known that this kind of deformation may modify the physical properties of layered 2D materials dramatically. For example, in AB-stacked bilayer graphene,

applying a perpendicular electric field can induce a gap opening in the electronic structure, and a subsequent compression of the interlayer spacing can widen the field-induced band gap (a 10% compression enhances the gap by 80%) [25]. Another example is layered MoS_2, which has been shown theoretically and experimentally to undergo a transition from a semiconductor to a metal with vertical pressure [26,27]. In general, decreasing the interlayer spacing may induce charge redistribution in layered 2D materials; it is therefore interesting and important to figure out whether the semiconducting layered $MoSi_2N_4$ and other members in the MA_2Z_4 (M = Ti/Cr/Mo, A = Si, Z = N/P) family are tunable under vertical strain.

In this work, we will solve this problem theoretically from first-principles density-functional theory calculations. Indeed, we show that the compressive strain can serve as an effective tool to tailor the electronic properties of bilayer $MoSi_2N_4$. Importantly, a semiconductor to metal transition is observed when the vertical compressive strain reaches 22%. Such a semiconductor to metal transition is the result of opposite energy shifts of states in two layers. The opposite energy shifts are further attributed to the enhanced interlayer interaction via asymmetric charge redistribution at the interface. Moreover, a simple estimation of the pressure demonstrates that such a transition in the MA_2Z_4 bilayer is feasible, as the applied pressure is on the order of a few to tens of gigapascals. Our theoretical investigations of the tunable electronic properties of bilayer MA_2Z_4 provide a guide for further experimental study and bring opportunities to build novel electromechanical devices from these newly synthesized 2D materials.

*yuj@shu.edu.cn
†s.yuan@whu.edu.cn

II. CALCULATION METHOD

Our calculations are performed using the projector augmented wave (PAW) method [28] implemented in the Vienna Ab initio Simulation Package (VASP) code [29]. The Perdew-Burke-Ernzerhof (PBE) form of the generalized gradient approximation exchange-correlation functional [30] with van der Waals corrections (vdW) [31,32] and the PAW pseudopotentials [28] are adopted. The cutoff energy is set to 500 eV after convergence tests. A Γ-centered Monkhorst-Pack k-point grid [33,34] of $9 \times 9 \times 1$ is used for relaxations, and a grid of $15 \times 15 \times 1$ is used for property calculations. In our current calculations, the total energy is converged to less than 10^{-6}eV, and the maximum force is less than 0.01 eV/Å during the optimization. A vacuum space along the z axis is larger than 20 Å to avoid spurious interactions. During the structure relaxation, the z coordinates of N atoms at the interface are fixed to ensure the layer spacing, and the z axis is fixed to ensure the thickness of the vacuum slab. The lattice relaxation is included for all strained samples.

III. RESULTS AND DISCUSSION

To verify the reliability of our result, we first perform first-principles calculations for the atomic and electronic structures of monolayer $MoSi_2N_4$. The optimized lattice constant is 2.91 Å, and the indirect band gap is 1.789 eV, which are in agreement with the values of 2.94 Å and 1.744 eV reported in a previous work [20]. With different stacking configurations, two $MoSi_2N_4$ monolayers can form five highly symmetric bilayer structures, namely, AB*, AC*, AB, AA, and AC (see the Supplemental Material [35]). Based on our calculated total energies of the ground states, the stability of these five structures follows the order of AA < AB*< AC*< AB < AC. Thus, we will take the most stable AC-stacked bilayers to discuss the related electronic properties in the rest of the paper.

The ball-stick structures of AC-stacked $MoSi_2N_4$ bilayers are presented in Figs. 1(a) and 1(b). The unit cell and unit vectors are marked by black vectors. As shown in Figs. 1(a) and 1(b), the Si atoms of the top monolayer are superimposed on the Mo2 atom of the bottom monolayer, and the Mo1 atom of the top monolayer is superimposed on the N1 and N4 atoms of the bottom monolayer, i.e., sitting above the hexagon centers of the bottom lattice. The optimized lattice constant for bilayer $MoSi_2N_4$ is the same as that of the monolayer. The layer distance between Mo1 and Mo2 atoms is 11.030 Å, much larger than that (6.23–6.54 Å) of bilayer transition metal dichalcogenides (TMDCs), such as MoS_2, WS_2, $MoSe_2$, and WSe_2 [36,37]. This suggests that the interlayer vdW interaction in bilayer $MoSi_2N_4$ is much weaker than bilayer TMDCs. Such an interlayer interaction is so weak that the band structure of bilayer $MoSi_2N_4$ is almost degenerate as two isolated monolayers in Fig. 1(c), except that there are negligible splittings of the highest (lowest) occupied (unoccupied) states along the Γ-K and Γ-M directions. For bilayer $MoSi_2N_4$, the valence band maximum (VBM) locates at the Γ point, about 0.271 eV higher than the highest occupied states at the K point, while the conduction band minimum (CBM) is at the K point, rendering an indirect band gap of 1.761 eV. When we take the spin-orbit coupling (SOC) into account, there will
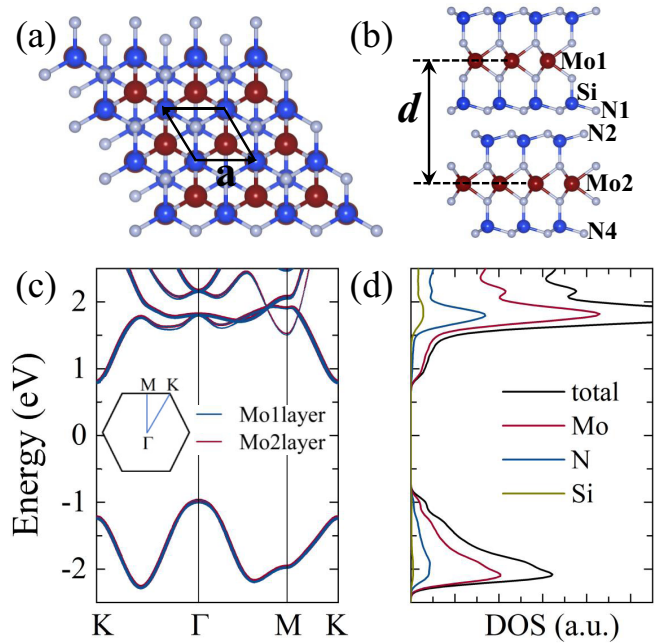
FIG. 1. (a) Top and (b) side views of atomic structure of bilayer $MoSi_2N_4$. The primitive cell and lattice vector **a** are labeled in (a). d is the interlayer distance between the top Mo1 and bottom Mo2 sublayers. (c) Projected band structure and (d) partial density of states of bilayer $MoSi_2N_4$. The inset in (c) shows the first Brillouin zone of bilayer $MoSi_2N_4$. The band gap center is set to be zero.

be a band splitting (0.141 eV) of the highest occupied states at the K point [35]. This spin-induced splitting is close to the value (0.149 eV) of MoS_2 [38,39]. However, no spin splitting is observed in the CBM at the K point in bilayer $MoSi_2N_4$. In Fig. 1(d), the projected density of states shows that both the VBM and CBM are dominated by the Mo atoms, with a partial contribution from N atoms but almost no contribution from Si atoms. With a more detailed analysis of the orbital contributions, the band edges are indeed mainly from the localized dz^2 orbitals of Mo atoms. It is worth noting that the observed SOC effects and orbital characters of the states at band edges are very similar to TMDC monolayers. Apart from the valence band splitting at the K point, the SOC effect does not modify the VBM and CBM of bilayer $MoSi_2N_4$, and, thus we will neglect this effect in the following sections.

Applying vertical strain is an effective way to modulate the electronic properties of layered materials. It can be realized by hydrostatic pressure [40], vacuum thermal annealing, nanomechanical pressures, or inserting hexagonal BN dielectric layers [41]. In our calculations, the vertical strain is implemented by the change in the interlayer distance and characterized by a quantity $\delta = (d\text{-}d_0)/d_0$, where d and d_0 are the vertical distances for strained and unstrained bilayers, respectively. Figure 2(a) shows the schematic diagram of bilayer $MoSi_2N_4$ under vertical strain perpendicular to the plane of the layer, where the arrows pointing inward and outward indicate compressive and stretched strains, respectively. Figure 2(b) depicts the evolutions of the total energy and band gap of bilayer $MoSi_2N_4$ under different vertical strains. When no strain is applied ($\delta = 0$), bilayer $MoSi_2N_4$ has an interlayer
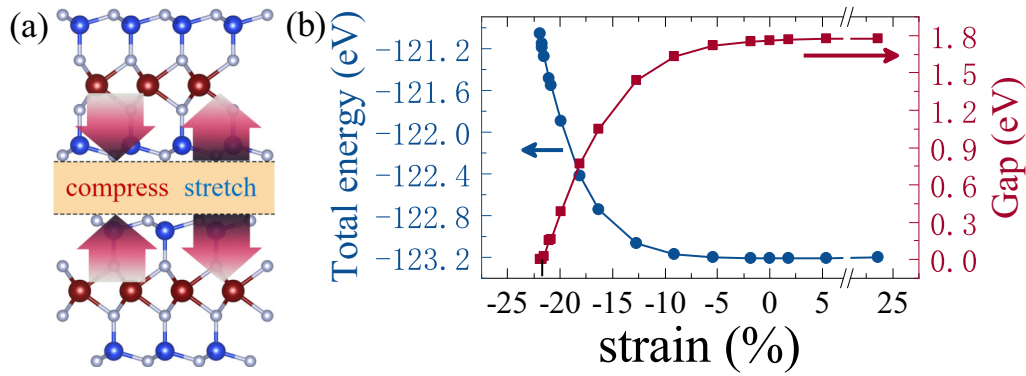
FIG. 2. (a) Schematic diagram of the bilayer $MoSi_2N_4$ under an external vertical strain along the direction perpendicular to the layer, where the arrows pointing inward and outward represent compressive and stretched strains, respectively. (b) The variation of total energy and band gap of bilayer $MoSi_2N_4$ as a function of the vertical strain. The zero band gaps are indicated by the black line.

distance of 11.030 Å, which is the most stable configuration with the lowest total energy. When the compression strain is applied within the range $\delta \geqslant -0.09$, the total energy remains almost the same, indicating that the interlayer interaction is too weak to affect the electronic properties. When further increasing the compressive strain, the total energy increases remarkably. Thus, the vertical strain with $\delta = -0.09$ can be regarded as the turning point where the interlayer interaction becomes strong and it cannot be neglected.

For the band gap, when the value of δ is above the threshold of -0.09, the indirect band gap is almost unchanged, similar to the trend of total energy. When δ is below the threshold, the band gap decreases significantly. This threshold strain corresponds to a vertical distance of 3.02 Å between inner N atoms of two monolayers, which is comparable to the layer spacing of layered TMDCs [42], black phosphorene (3.21 Å) [43], and borophene (3.07 Å) [44]. In layered TMDCs, the interlayer interaction does affect their electronic structures greatly, changing the band gap from direct in a monolayer to indirect in multilayers [19,45,46]. Here, if we continuously increase the compressed strain in bilayer $MoSi_2N_4$, an electronic phase transition from semiconductor to metal is finally observed when the value of δ reaches -22%. The corresponding vertical compressive pressure P is 18.66 GPa, which is estimated in terms of $P = (E - E_0)/A(d_0 - d)$ [42,47], where E and E_0 are total energies at layer distances d and d_0 (equilibrium) and A is the area of the cell. Such a transition pressure is on the same order as bilayer TMDCs (5.10–16.28 GPa) [42]. Generally, the electronic phase transition is accompanied by a structural transition under high pressure [42]. However, for bilayer $MoSi_2N_4$ under the transition pressure, the AC-stacked mode is still found to be the most stable one among the five considered structures, indicating that there is no structural transition during the strain process. This is consistent with the excellent ambient stability observed in layered $MoSi_2N_4$ in experiments [20]. Our predicted transition pressure of bilayer $MoSi_2N_4$ can be realized by hydrostatic pressure [40], making it attractive for electromechanical applications.

To ensure the stability of compressed $MoSi_2N_4$ bilayer, we first performed phonon calculations of the atomic structure with critical transition strain. The phonon spectrum in Fig. 3(a) shows no imaginary frequencies, indicating kinetic

stability of the bilayer under huge compression. Slightly different from the phonon spectrum of unstrained bilayer $MoSi_2N_4$ [35], some degenerate phonon branches are lifted as a result of enhanced interlayer interaction. As phonon calculations do not take temperature into account, we next adopt *ab initio* molecular dynamics (AIMD) simulations to confirm the thermal stability of strained $MoSi_2N_4$ bilayers in Fig. 3(b). It is found that the geometry of the AC-stacked $MoSi_2N_4$ bilayer is well preserved at room temperature. When the temperature increases up to 800 K [35], the geometry of the AC-stacked $MoSi_2N_4$ bilayer is still retained. The phonon spectrum and AIMD results manifest the excellent ambient stability of bilayer $MoSi_2N_4$ under vertical compression.

Because the band gap varies significantly within the range $\delta \leqslant -0.09$ in Fig. 2(b), we will focus on the vertical compressive strains in this range. In Fig. 4, we present the band structures of bilayer $MoSi_2N_4$ under four representative compressive strains from 9% to 23%. As a result of $\delta = 9\%$, shown in Fig. 4(a), notable changes appear in the electronic structure of bilayer $MoSi_2N_4$ in which there are slight splittings of energy bands. These band splittings become more evident with increasing compressive strain (see the changes in δ from 9% to 16% and 22%). Here, we can quantitatively define the rigid energy shift as the energy difference between VB1 (CB1) and VB2 (CB2) at the K (Γ) point as labeled in Fig. 4(b). When the compressive strain increases from 9% to 23%, the energy shift increases significantly from 0.116 to 1.605 eV. More importantly, the energy dispersion of each individual band remains almost the same during the compression process. As a result, the charge carrier will maintain its small effective mass and high mobility, similar to their values (270–1200 cm^2 V^{-1} s^{-1}) [20] in the pristine monolayer. If we inject an electron or hole into a strained bilayer, the electron or hole will occupy the energy band of CB1 or VB1 separately; thus, a switchable tunnel for electron or hole transport can be realized in separate layers. Carrier injection thus can be used to effectively tune the transport properties of strained $MoSi_2N_4$ bilayers. On the other hand, with increasing compressive strain, both the VBM and CBM are driven continuously toward the Fermi level and thus reduce the energy band gap. The indirect band gap of bilayer $MoSi_2N_4$ decreases from 1.633 to 0 eV when the compressive strain increases from 9% to 22%. After the com-
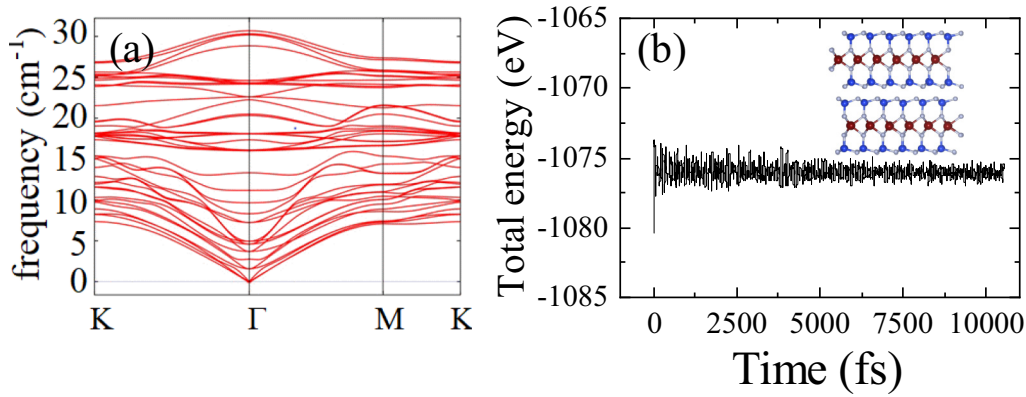
FIG. 3. (a) Phonon dispersions of bilayer $MoSi_2N_4$ at vertical compressive strain of 22%. (b) Evolution of total energy versus simulation time in AIMD for AC-stacked bilayer $MoSi_2N_4$ under vertical compressive strain of 22% at room temperature. The inset in (b) is a snapshot of the final equilibrium structures.

pression reaches the critical value of 22%, the metallic feature appears in the band structure, as shown in Figs. 4(c) and 4(d), where $\delta \geqslant 22\%$, indicating clearly a robust semiconductor to metal phase transition.

In order to find the origin of this semiconductor to metal phase transition, we extract the partial density of states (PDOS) of bilayer $MoSi_2N_4$ with or without strain. As we have already shown that the band edges of bilayer $MoSi_2N_4$ are dominated by Mo states, we thus focus on the states of Mo atoms in the two layers. As shown in Fig. 5(a), the calculated PDOSs of two Mo atoms from different layers in pristine $MoSi_2N_4$ bilayers are totally degenerate because of the symmetric atomic structures of the two layers. Under a vertical compressive strain of 22%, the overall shapes of the PDOS from two Mo are preserved, but they have opposite energy shifts, and there is an overlap of the highest valence state of one Mo and the lowest conduction state of the other, as shown in Fig. 5(b). This overlap of Mo states agrees with the semiconductor to metal transition in bilayer $MoSi_2N_4$ under the critical strain of 22%. If we make an analysis of the PDOS from N atoms in different layers, although their contributions to the states at the band edges are much smaller, the spectrum shift of each N atom is similar to the Mo atom within the

same layer. Furthermore, there is a significant enhancement of PDOS of N1 and N2 atoms, indicating an enhancement of interlayer interaction between the p_z orbitals of N atoms in the inner sublayers.

The opposite energy shift of the PDOS indicates a possible strain-induced change in the electric potentials of these atoms. We thus calculate the plane-averaged charge density difference $\Delta\rho(z)$ along the vertical direction (z axis) for $MoSi_2N_4$ bilayers with different strains and plot the results in Fig. 6. Here, $\Delta\rho(z)$ is calculated by the charge density difference between the bilayer and two noninteracting monolayers. A positive $\Delta\rho(z)$ indicates the accumulation of the charge density, while a negative value means the depletion. For unstrained bilayer $MoSi_2N_4$, $\Delta\rho(z)$ is almost zero for all z coordinates, suggesting no charge transfer between layers. This is also consistent with the observed very weak interlayer vdW interaction in pristine bilayer $MoSi_2N_4$. For strained bilayer $MoSi_2N_4$, we see clearly that changes in $\Delta\rho(z)$ are totally different on the two sides of the interface. Although in both layers there are fluctuations in $\Delta\rho(z)$, clearly, on one side the overall values of $\Delta\rho(z)$ are negative, and on the other side they are positive, indicating the charge transfer between the two layers. The amount of charge transfer Q, obtained by
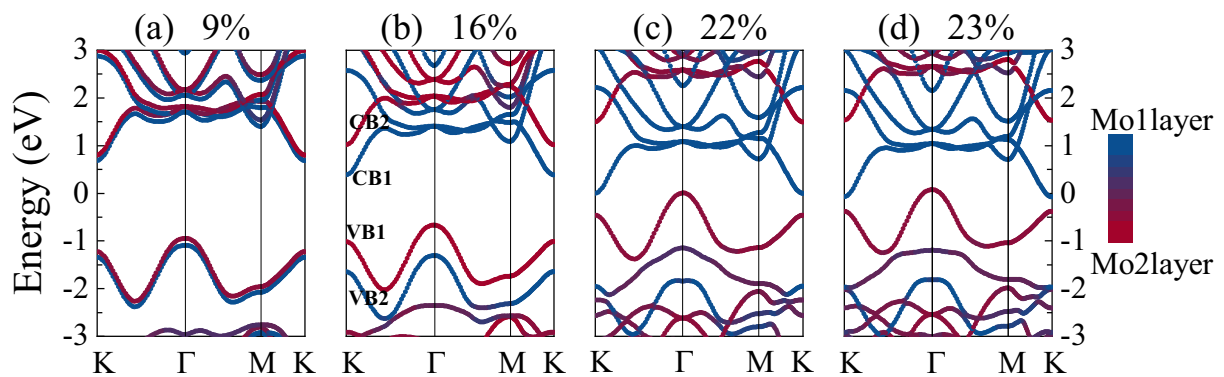
FIG. 4. Band structures of bilayer $MoSi_2N_4$ under vertical compressive strains from 9% to 23%. Blue (red) indicates the orbital contribution to the band structure from the Mo1 layer (Mo2 layer), and the intermediate color means that the state is contributed by the two layers. All bands are shifted to align the deep Mo $5s$ state. Two conduction bands (CB1 and CB2) and two valence bands (VB1 and VB2) are labeled in (b).
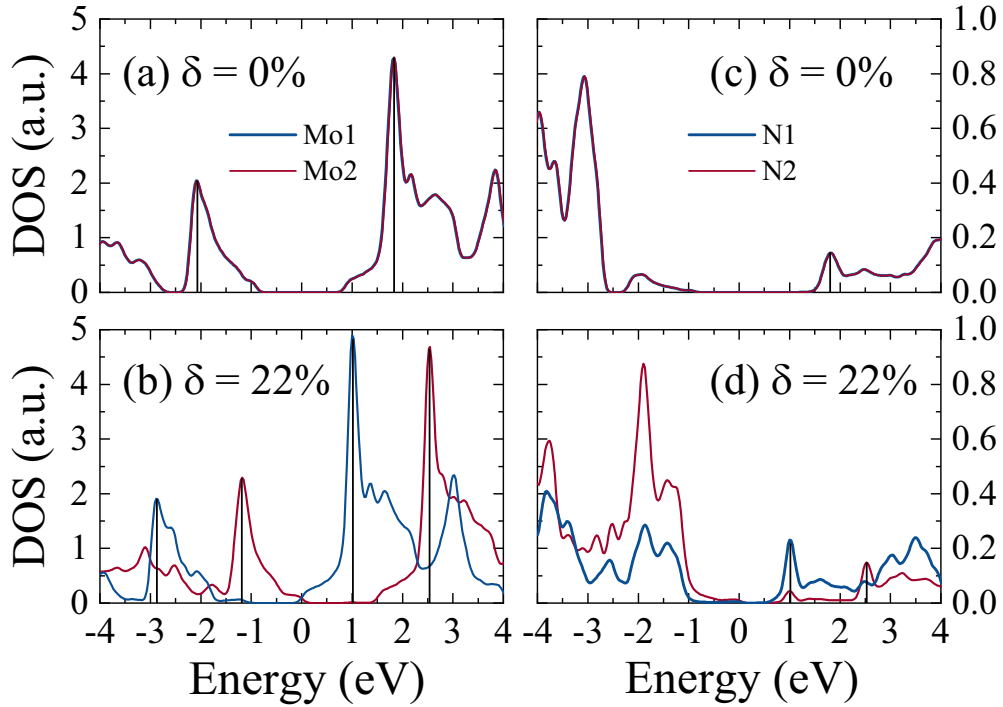
FIG. 5. Partial density of states (PDOS) of Mo1, Mo2, N1, and N2 atoms (as labeled in Fig. 1) in bilayer $MoSi_2N_4$ with or without strain. All the energies are shifted to align the deep Mo 5s state.

the integral of $\Delta\rho(z)$ along one side of the interface, increases monotonically as compression strain increases. Furthermore, if we calculate the ratio between Q and band gap reduction for different strains, we obtain a set of values around 0.035. This correlation between Q and the reduced energy gap indicates that the asymmetric charge redistribution at the interface

causes the opposite energy shift of the two layers and, subsequently, the semiconductor to metal phase transition at the critical compressive strain.

To get a general conclusion, we study numerically the strain-induced semiconductor to metal transition in other MA_2Z_4 bilayers and summarize their structural parameters and transition pressures in Table I. Owing to the weak interlayer interaction, the interlayer separation of the unstrained bilayer MA_2Z_4 is around 4.02 Å, larger than those (3.11–3.39 Å) of bilayer TMDCs [42]. By increasing the vertical compressive strain, the interlayer separation decreases accordingly. Under the transition strain, all considered MA_2Z_4

FIG. 6. Plane-averaged charge density difference $\Delta\rho(z)$ of bilayer $MoSi_2N_4$ under vertical compressive strain from 0% to 22%. The top panel is a three-dimensional charge density difference under a strain of 22%, and the isosurface value is 0.002 e/Å^3. The green and yellow areas represent electron accumulation and depletion, respectively.

TABLE I. Distance between two Z atoms from different layers in pristine bilayer MA_4Z_2 and estimated pressure required for realizing the semiconductor to metal transition. We also list the vertical separation between interlayer anion atoms and the corresponding pressure for semiconductor to metal transition in some AB-stacked TMDCs for comparison [42].

	Bilayer separation at transition (Å)	Bilayer separation at equilibrium (Å)	Transition pressure (Gpa)
$MoSi_2N_4$	1.62	4.02	18.66
$MoSi_2P_4$	2.42	4.02	2.38
$CrSi_2N_4$	2.62	4.03	2.18
$TiSi_2N_4$	1.20	4.04	32.04
MoS_2	2.14	3.11	8.52
$MoSe_2$	2.23	3.19	8.37
$MoTe_2$	2.69	3.37	5.10
WS_2	1.80	3.39	16.28
WSe_2	2.21	3.35	15.83

bilayers change from semiconductor to metal, and the interlayer separation ranges from 1.62 to 2.62 Å, close to the value (1.80–2.69 Å) of bilayer TMDCs at the transition point [42]. The estimated transition pressure ranges from 2.18 GPa in bilayer $CrSi_2N_4$ to 18.66 GPa in bilayer $MoSi_2N_4$, which is on the same order as that (5.10–19 GPa) in well-studied layered TMDCs [26,42]. Particularly, bilayer $CrSi_2N_4$ and $MoSi_2P_4$ have very small transition pressures (2.18–2.38 GPa) compared to other studied MA_2Z_4. Our calculations suggest that the strain-induced semiconductor to metal transition in semiconducting bilayer MA_2Z_4 can be easily realized experimentally.

To further validate the reliability of our conclusion, we discuss the band gap revision and layer effects on $MoSi_2N_4$. Because standard PBE calculations usually underestimate the band gap, we thus perform Heyd-Scuseria-Ernzerhof calculations with hybrid functionals to reproduce the semiconductor to metal transition, and we found that the transition occurs with a bit larger strain of around 24%. We also check the layer effects on the semiconductor to metal transition in layered $MoSi_2N_4$. Our extended calculations show that the semiconductor to metal transition also appears in four-layer $MoSi_2N_4$; the transition strain becomes smaller, around 18%, and the corresponding pressure is 15.03GPa, which is also smaller than that of stacked bilayer. Therefore, we expect that similar transitions can be observed in other multilayer and bulk MA_2Z_4 with experimentally reachable pressures.

IV. CONCLUSION

In conclusion, we have studied the electronic properties of MA_2Z_4 (M = Ti/Cr/Mo, A = Si, Z = N/P) bilayers under different vertical strains using first-principles density-functional theory calculations. Taking the recently fabricated $MoSi_2N_4$ as an example, we showed that the electronic properties of bilayer $MoSi_2N_4$ can be effectively tuned by the vertical compressive strain. To be more exact, with increasing compressive strain, the band gap of bilayer $MoSi_2N_4$ monotonically decreases and finally closes when the vertical strain reaches 22%. This is a result of the opposite energy shift of the states in different layers, which is driven by the asymmetric charge redistribution on the inner Z-Z sublayer at the interface. We further confirmed that a similar semiconductor to metal transition exists in other strained MA_2Z_4 bilayers, and the estimated transition pressure to realize such a transition ranges from 2.18 GPa in $CrSi_2N_4$ to 32.04 GPa in TiSi2N4. Our theoretical predictions provide guidance for further exploring the strain-tunable electronic properties of layered semiconducting MA_2Z_4.

[1] K. S. Novoselov, A. K. Geim, S. V. Morozov, D. Jiang, Y. Zhang, S. V. Dubonos, I. V. Grigorieva, and A. A. Firsov, Science **306**, 666 (2004).

[2] K. S. Novoselov, D. Jiang, F. Schedin, T. Booth, V. Khotkevich, S. Morozov, and A. K. Geim, Proc. Natl. Acad. Sci. USA **102**, 10451 (2005).

[3] K. S. Novoselov, A. K. Geim, S. V. Morozov, D. Jiang, and M. I. Katsnelson, Nature (London) **438**, 197 (2005).

[4] A. K. Geim and K. S. Novoselov, Nat. Mater. **6**, 183 (2007).

[5] K. S. Novoselov, Z. Jiang, Y. Zhang, S. Morozov, H. L. Stormer, U. Zeitler, J. Maan, G. Boebinger, P. Kim, and A. K. Geim, Science **315**, 1379 (2007).

[6] T. G. Pedersen, C. Flindt, J. Pedersen, N. A. Mortensen, A.-P. Jauho, and K. Pedersen, Phys. Rev. Lett. **100**, 136804 (2008).

[7] Y. Zhang, Y.-W. Tan, H. L. Stormer, and P. Kim, Nature (London) **438**, 201 (2005).

[8] S. Y. Zhou, G.-H. Gweon, A. V. Fedorov, P. N. First, W. A. de Heer, D.-H. Lee, F. Guinea, A. H. Castro Neto, and A. Lanzara, Nat. Mater. **6**, 770 (2007).

[9] C. Ataca, H. Sahin, and S. Ciraci, J. Phys. Chem. C **116**, 8983 (2012).

[10] W. Wu, P. Lu, Z. Zhang, and W. Guo, ACS Appl. Mater. Interfaces **3**, 4787 (2011).

[11] J. Yu and W. Guo, J. Phys. Chem. Lett. **4**, 1856 (2013).

[12] Z. Zhang, X. Liu, B. I. Yakobson, and W. Guo, J. Am. Chem. Soc. **134**, 19326 (2012).

[13] H. L. Zhuang and R. G. Hennig, Appl. Phys. Lett. **101**, 153109 (2012).

[14] M. Chhowalla, H. S. Shin, G. Eda, L.-J. Li, K. P. Loh, and H. Zhang, Nat. Chem. **5**, 263 (2013).

[15] C. R. Dean, A. F. Young, I. Meric, C. Lee, L. Wang, S. Sorgenfrei, K. Watanabe, T. Taniguchi, P. Kim, and K. L. Shepard, Nat. Nanotechnol. **5**, 722 (2010).

[16] R. Ganatra and Q. Zhang, ACS Nano **8**, 4074 (2014).

[17] L. Li, Y. Yu, G. J. Ye, Q. Ge, X. Ou, H. Wu, D. Feng, X. H. Chen, and Y. Zhang, Nat. Nanotechnol. **9**, 372 (2014).

[18] G. Lu, T. Wu, Q. Yuan, H. Wang, H. Wang, F. Ding, X. Xie, and M. Jiang, Nat. Commun. **6**, 1 (2015).

[19] K. F. Mak, C. Lee, J. Hone, J. Shan, and T. F. Heinz, Phys. Rev. Lett. **105**, 136805 (2010).

[20] Y. L. Hong, Z. Liu, L. Wang, T. Zhou, and W. Ren, Science **369**, 670 (2020).

[21] M. Naguib, V. N. Mochalin, M. W. Barsoum, and Y. Gogotsi, Adv. Mater. **26**, 992 (2013).

[22] X. Zhang, Z. Ma, X. Zhao, Q. Tang, and Z. Zhou, J. Mater. Chem. A **3**, 4960 (2015).

[23] Z. Wang, V. Kochat, P. Pandey, S. Kashyap, S. Chattopadhyay, A. Samanta, S. Sarkar, P. Manimunda, X. Zhang, and S. Asif, Adv. Mater. **29**, 1700364 (2017).

[24] J. Xie, S. Li, X. Zhang, J. Zhang, R. Wang, H. Zhang, B. Pan, and Y. Xie, Chem. Sci. **5**, 4615 (2014).

[25] Y. Guo, W. Guo, and C. Chen, Appl. Phys. Lett. **92**, 243101 (2008).

[26] A. P. Nayak, S. Bhattacharyya, J. Zhu, J. Liu, X. Wu, T. Pandey, C. Jin, A. K. Singh, D. Akinwande, and J.-F. Lin, Nat. Commun. **5**, 3731 (2014).

[27] Z.-H. Chi, X.-M. Zhao, H. Zhang, A. F. Goncharov, S. S. Lobanov, T. Kagayama, M. Sakata, and X.-J. Chen, Phys. Rev. Lett. **113**, 036802 (2014).

[28] P. E. Blöchl, Phys. Rev. B **50**, 17953 (1994).

[29] G. Kresse and J. Furthmüller, Phys. Rev. B **54**, 11169 (1996).

[30] J. P. Perdew, K. Burke, and M. Ernzerhof, Phys. Rev. Lett. **77**, 3865 (1996).

[31] J. Klimeš, D. R. Bowler, and A. Michaelides, Phys. Rev. B **83**, 195131 (2011).

[32] M. Dion, H. Rydberg, E. Schröder, D. C. Langreth, and B. I. Lundqvist, Phys. Rev. Lett. **92**, 246401 (2004).

[33] J. D. Pack and H. J. Monkhorst, Phys. Rev. B **16**, 1748 (1977).

[34] H. J. Monkhorst and J. D. Pack, Phys. Rev. B **13**, 5188 (1976).

[35] See Supplemental Material at http://link.aps.org/supplemental/10.1103/PhysRevB.103.085124 for details regarding the atomic configuration, calculated total energy, simulations for bilayer $MoSi_2N_4$, and the computational details.

[36] S. Gao, L. Yang, and C. D. Spataru, Nano Lett. **17**, 7809 (2017).

[37] J. He, K. Hummer, and C. Franchini, Phys. Rev. B **89**, 075409 (2014).

[38] D. Xiao, G.-B. Liu, W. Feng, X. Xu, and W. Yao, Phys. Rev. Lett. **108**, 196802 (2012).

[39] Y. Wang, L. Deng, Q. Wei, Y. Wan, Z. Liu, X. Lu, Y. Li, L. Bi, L. Zhang, and H. Lu, Nano Lett. **20**, 2129 (2020).

[40] L. Fu, Y. Wan, N. Tang, Y.-m. Ding, J. Gao, J. Yu, H. Guan, K. Zhang, W. Wang, and C. Zhang, Sci. Adv. **3**, e1700162 (2017).

[41] K. D. Pham, N. N. Hieu, H. V. Phuc, I. Fedorov, C. Duque, B. Amin, and C. V. Nguyen, Appl. Phys. Lett. **113**, 171605 (2018).

[42] S. Bhattacharyya and A. K. Singh, Phys. Rev. B **86**, 075454 (2012).

[43] R. Fei and L. Yang, Nano Lett. **14**, 2884 (2014).

[44] H. Zhong, K. Huang, G. Yu, and S. Yuan, Phys. Rev. B **98**, 054104 (2018).

[45] A. Splendiani, L. Sun, Y. Zhang, T. Li, J. Kim, C.-Y. Chim, G. Galli, and F. Wang, Nano Lett. **10**, 1271 (2010).

[46] Y. Zhang, T.-R. Chang, B. Zhou, Y.-T. Cui, H. Yan, Z. Liu, F. Schmitt, J. Lee, R. Moore, and Y. Chen, Nat. Nanotechnol. **9**, 111 (2014).

[47] L.-Y. Gan, Q. Zhang, Y. Cheng, and U. Schwingenschlögl, Phys. Rev. B **88**, 235310 (2013).